University of Szeged
Graduate School of Pharmaceutical Sciences

Educational Program: Pharmaceutical Technology
Head: Prof. Dr. habil. Ildikó Csóka, PhD

Institute of Pharmaceutical Technology and Regulatory Affairs
Supervisors: Dr. habil. Géza Regdon jr. and Dr. habil. Tamás Sovány

Yousif Hamed Elneil Yousif Ibrahim

Development and Characterization of Lysozyme Pellets Prepared by Extrusion and Spheronization Method

Final Exam Committee:

Head:	**Prof. Dr. Piroska Révész,** DSc, University of Szeged, Faculty of Pharmacy, Institute of Pharmaceutical Technology and Regulatory Affairs
Members:	**Prof. Dr. Ildikó Bácskay**, PhD, University of Debrecen Faculty of Pharmacy, Department of Pharmaceutical Technology
	Dr. Zoltán Aigner, PhD, University of Szeged, Faculty of Pharmacy, Institute of Pharmaceutical Technology and Regulatory Affairs

Reviewer Committee:

Head:	**Prof. Dr. István Zupkó**, DSc, University of Szeged Faculty of Pharmacy, Institute of Pharmacodynamics and Biopharmacy
Reviewers:	**Prof. Dr. Ildikó Bácskay**, PhD, University of Debrecen Faculty of Pharmacy, Department of Pharmaceutical Technology
	Dr. Ferenc Fenyvesi, PhD, University of Debrecen Faculty of Pharmacy, Department of Pharmaceutical Technology
Members:	**Dr. Andrea Vasas**, PhD, University of Szeged Faculty of Pharmacy, Department of Pharmacognosy
	Dr. Gerda Szakonyi, PhD, University of Szeged Faculty of Pharmacy, Institute of Pharmaceutical Analysis

Szeged
2021

1. INTRODUCTION

The oral route of drug administration is more preferable to the other routes as a result of good patient compliance and formulation adjustability. Among orally ingested medications; multiparticulate delivery systems such as pellets possessed increased attention and applications due to several advantages such as lower gastrointestinal tract (GIT) irritation, more even and predictable transportation and distribution in the GIT regardless of the nutritional status, flexibility of mixing units with different release behaviors; low risk of dose dumping, spherical shape enabling the coating/subcoating process to be performed efficiently and hence setting the release design. In addition, the incorporation of a mucoadhesive polymer could add extra innovative properties such as precise site-specific delivery, long residence time at the absorptive tissues, and hence improved bioavailability of the loaded drug.

Accordingly, pellets may offer a promising alternative for the delivery of therapeutic proteins (TP) which require the incorporation of safe and efficient protease inhibitor (PI), permeation enhancer (PE), and conformation stabilizers. Furthermore, intensive investigation of the material characteristics and the effect of different processing parameters on the targeted product profile (TPP) could be helpful tools in identifying the optimal design space of their production.

2. AIMS

The main aim of this study was the development and optimization of a system for lysozyme delivery, based on pellets prepared by extrusion/spheronization. The main optimization parameters were preserving the biological activity during and after production and acquiring adequate sphericity and hardness for the subsequent coating processes. The secondary aim was to design and develop citric acid (CA)-based chitosan films and thoroughly investigate their properties in comparison to acetic acid (AA)-based films as a reference, the best composites were screened for the subcoating process based on their obtained properties. These aims were based on the following hypotheses:

I. Material attributes may affect the optimal design space of pelletization, and thermomechanical shocks may negatively affect the biological activity of the finished product.
II. The knowledge of the distribution of relative humidity (RH%) and temperature (T) may help to optimize the processing parameters. Therefore, wetting was performed in a high-

shear granulator constructed with a specially designed Teflon-made chamber to monitor the change of RH% and T.

III. Chitosan citrate may represent a novel well-shielding multifunctional protein carrier system, as it provides a long residence time at the targeted absorptive tissues and concurrently offers PI and PE effects in a localized pattern.

3. MATERIALS

For pelletization; two brands of the hen egg-white lysozyme were involved; spray-dried (Lysoch-40000, Handary SA, Brussels, Belgium), described as "lyso-1" and lyophilized (CAT. HY-B2237/CS-7671, MedChemExpress, Hungary), described as "lyso-2", were involved as model antimicrobial/anti-inflammatory enzyme proteins. Spray-dried mannitol (SDM) (Hungaropharma Ltd., Budapest, Hungary) and crystalline mannitol (CM) "Pearlitol SD-200" (Hungaropharma Ltd., Budapest, Hungary), were utilized as conformation stabilizers. Microcrystalline cellulose (MCC, Avicel pH 101, FMC Biopolymer, Philadelphia, USA) was used as pellet former and drug carrier. Lyophilized *Micrococcus lysodeikticus* (Sigma-Alorich, USA) was used as a model Gram-positive bacteria for biological activity investigation of the prepared pellets.

For the development and characterization of the films; chitosan 80/1000 (Heppe Medical Chitosan GmbH., Germany) was involved as a film-forming mucoadhesive polymer. Acetic acid (AA) 99.8% (Sigma-Aldrich, Germany) and citric acid monohydrate (CA) (Molar Chemicals Kft, Hungary) were primarily used as solubility enhancer for chitosan. Glycerol (G), propylene glycol (PG) (Hungopharma Rt., Hungary), and polyethylene glycol 400 (PEG-400) (Sigma-Aldrich, Germany) were used as plasticizers. Mucin 75-95 % (Roth, Germany) was used as a substrate for the mucoadhesivity investigation, and diiodomethan (VWR Prolabo, USA) was used as a non-polar liquid for surface free energy (SFE) investigation.

4. METHODS

4.1. Design space of pelletization

4.1.1. Design of experiments

The experimental design was made according to 2^3 full factorial design with a central point. The impeller speed (x_1), liquid addition rate (x_2) and extrusion speed (x_3) were studied as independent factors, while the properties of the pellets were settled as optimization parameters. The analysis was made by using Statistica v. 13.5. Software (Tibco Statistica Inc, Palo Alto, CA, USA).

4.1.2. Scanning electron microscopy

The morphology and size of the raw materials were investigated by Scanning Electron Microscope (SEM) (Hitachi 4700, Hitachi Ltd., Tokyo, Japan).

4.1.3. Homogenization

100 g of powder mixtures (Table 1) were homogenized in a Turbula mixer (Willy A. Bachofen Maschienenfabrik, Basel, Switzerland) for 10 minutes.

Table1. Composition of the mixtures

Excipients	C1 (g)	C2 (g)	C3 (g)
Lyso-1	10	10	-
Lyso-2	-	-	10
CM	40	-	40
SDM	-	40	-
MCC	50	50	50

4. 1.4. Estimation of water quantity

The exact quantity of the granulating liquid is critical. Accordingly, Enslin number has been measured to determine the water absorbed by 1 g of the powder mixture (ml/g).

4.1.5. Wet granulation

The homogenized mixtures of the powder samples were wetted and kneaded in a ProCepT 4M8 high shear granulator (ProCepT nv. Zelzate, Belgium). The processing parameters are illustrated below in Table 2. The wet granulation and kneading were performed in a specially designed Teflon-granulation chamber (Opulus Ltd., Szeged, Hungary) equipped with seven RH and T sensors as shown in Figure1.

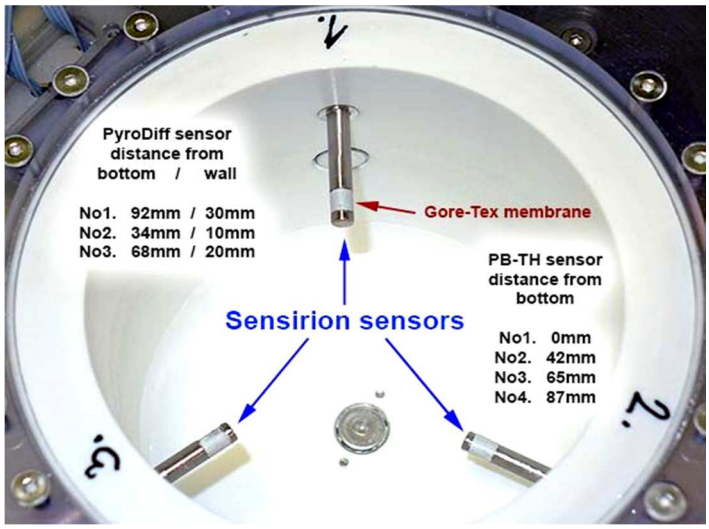

Figure 1. Kneading chamber showing the configuration of immersed (PyroDiff®) and PyroButton-TH® sensors

Table 2. Processing parameters of the kneading, extrusion and spheronization

Kneading	**Process-1**		**Process-2**		**Process-3**		**Process-4**		**Process-5**
Impeller speed (x_1)	500 (-1)		500 (-1)		1500 (+1)		1500 (+1)		1000 (0)
Liquid addition rate ml/minute (x_2)	5 (-1)		10 (+1)		5 (-1)		10 (+1)		7.5 (0)
Purified H_2O (ml)	60		60		60		60		60
Chopper speed	500		500		500		500		500
Extr./spheron.									
Extrusion speed (x_3)	70 (-1)	120(+1)	70 (-1)	120(+1)	70 (-1)	120(+1)	70 (-1)	120(+1)	95 (0)
Spher. speed (rpm)	2000	2000	2000	2000	2000	2000	2000	2000	2000
Spher. time (minute)	1	1	1	1	1	1	1	1	1
Spher. amount (g)	17	17	17	17	17	17	17	17	17
Sample code	**LysC-11**	**LysC-12**	**LysC-21**	**LysC-22**	**LysC-31**	**LysC-32**	**LysC-41**	**LysC-42**	**LysC-c**

***C**: referring to the composition; 1, 2 and 3 for the first (C1), second (C2) and third (C3) composition, respectively

4.1.6. Extrusion and spheronization

Extrusion was made by a single-screw extruder (Caleva Process Solutions Ltd., Sturminster Newton, UK). The extruded samples were spheronized by Caleva MBS spheronizer (Caleva Process Solutions Ltd., Sturminster Newton, UK), and the processing conditions are shown above in Table 2.

4.1.7. Pellet's activity measurement

The biological activity (y_1) of the prepared pellets was measured via the degradation of lyophilized *Micrococcus lysodeikticus* (n=3), by using a Genesys 10 S UV-VIS Spectrometer (ThermoScientific, Waltham, MA, USA).

4.1.8. Hardness and deformation

The deformation force (y_2) and pattern were investigated by a custom-made texture analyzer; the equipment and its software were developed at the University of Szeged, Institute of Pharmaceutical Technology and Regulatory Affairs, (n= 20).

4.1.9. Moisture content

The moisture content (y_3) of the prepared pellets was measured by using Mettler-Toledo HR73 (Mettler-Toledo Hungary Ltd., Budapest, Hungary) halogen moisture analyzer at 105ºC, (n= 3).

4.1.10. Size and shape study

The size and shape (y_4 and y_5) were investigated by using a stereomicroscope and a ring light with a cold light source (Carl Zeiss, Oberkochen, Germany). The images (n=100) were analyzed with a Leica Quantimet 500 C image analysis software (Leica Microsystems, Wetzlar, Germany).

4.2. Design of chitosan films

4.2.1. Preparation method

Chitosan films were prepared by the solvent casting method, by dissolving the polymer (2 w/v %) in aqueous AA solution (2 v/v %) as a reference, and with the use of CA (2.5, 3, 3.5, 4, 5, and 7 w/v %). Plasticizers were added to AA, CA 2.5% and CA 7%-based solutions in approx. five to ten times excess (5 w/v% and 10 w/v %) compared to the polymer. The exact compositions of the prepared solutions/films are shown below in Table 3.

Table 3. Composition of prepared citric acid (CA)- and acetic acid (AA)-based solutions/films

Plasticizer	w/v%	Chitosan w/v%	CA w/v%	CA w/v%	CA w/v%	CA w/v%	CA w/v%	CA w/v%	AA v/v%
-	0	2	2.5	3	3.5	4	5	7	2
G	5	2	2.5	-	-	-	-	7	2
	10	2	2.5	-	-	-	-	7	2
PG	5	2	2.5	-	-	-	-	7	2
	10	2	2.5	-	-	-	-	7	2
PEG-400	5	2	2.5	-	-	-	-	7	2
	10	2	2.5	-	-	-	-	7	2

A magnetic stirrer was used to obtain 100 mL homogeneous solutions. A portion (~ 25 mL) of each solution was taken for the minimum film forming temperature (MFFT) testing, while the remaining amount was cast into gasket rings (19.635 cm^2 x 0.5 cm) as 10 g/ring.

4.2.2. MFFT investigation

MFFT was investigated with a Rhopoint MFFT-60 Bar tester (Rhopoint, UK) at the temperature range of 15–60 ºC (n=5).

4.2.3. Infrared Spectroscopy

The infrared spectra for the films and the other excipients were obtained by using an FT-IR (Avatar 330 FT-IR ThermoScientific, USA) apparatus coupled with a Zn/Se HATR (horizontal attenuated total reflectance) accessory, by applying CO2 and H2O corrections.

4.2.4. Film thickness

The thickness of the films was measured at 10 randomly selected points on each film by using a screw micrometer (Mitutoyo Co. Ltd, Japan).

4.2.5. Hardness and mucoadhesion investigations

Hardness and mucoadhesivity were investigated by the same equipment prescribed in section (4.1.8) but, with a different assembling of the moving probe and sample holder. A mucin

solution of 1mg/ml was used as a reagent for the determination of the mucoadhesivity force (n= 10 for the hardness, and n=5 for the mucoadhesivity).

4.2.6. Calculation of SFE

SFEs were calculated indirectly from the means of the contact angles (Θ) of water and diiodomethane by using the optical contact angle measuring apparatus (OCA20-DataPhysics Instrument GmbH, Filderstadt, Germany), via the application of the sessile drop method (n= 10).

4.2.7. Thermal analysis

Thermal gravimetric analysis (TGA) and differential scanning calorimetry (DSC) were carried out by using TG/DSC1 equipment (Mettler-Toledo Inc., Switzerland). The heating was at a constant rate of $10°C \cdot min^{-1}$. The mass of the samples was 10±2 mg.

4.2.8. Statistical analysis

The gathered data were analyzed according to a factorial ANOVA method using Tibco Statistica v13.1 (Statsoft, Tulsa, OK, USA) software.

5. RESULTS AND DISCUSSION

5.1. Investigation of the change in T and RH%

The variation of the recorded values was attributed to the location of the sensor and its distance from the impeller rotational axis, as illustrated above in Fig. 1. As expected, at a lower (-1) level of impeller speed, the internal chamber temperature was relatively low and constant throughout the wet kneading period, which is advantageous for processing thermolabile molecules. Under these conditions, the liquid addition rate has less impact on the temperature value, as demonstrated in Figure 2.

When operating at a high (+1) level of impeller speed (processes 3 and 4), the liquid addition rate exhibited more considerable influence on the temperature distribution inside the chamber, although it was only partially able to compensate for the temperature elevation which was induced by mechanical friction between the kneaded mass, impeller and chamber wall. Overall, the temperature change mostly depends on impeller speed and exhibited a linear relation with the investigated parameters (Eq. 1).

$$y_{\Delta T} = 15.409 + \mathbf{10.643}x_1 - 3.176x_2 - 1.633x_1x_2 \quad (1)$$

$R^2 = 0.99836$ Adj $R^2 = 0.99344$ MS Residual = 0.828245

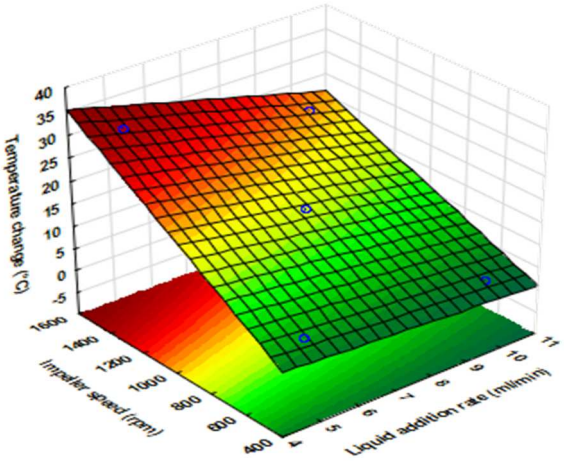

Figure 2. Temperature change in the kneading phase

In contrast, the variation of system RH did not follow the expectations since the increasing liquid addition rate resulted in a reduced increment of RH. This unexpected phenomenon may be due to the insufficient equilibration time of MC% on the solid-air interface. The highest increment in the system RH% values was recorded in the central point (Figure 3). The low adj. R^2 and the high curvature coefficient of the corresponding Eq. (2) indicates a poor model quality, which may be due to a strong nonlinear relationship between the tested factors and RH%.

$$y_{RH\%}=53.6158-2.3742x_1-2.2925x_2 \qquad (2)$$

R^2= 0.80017 Adj R^2=0.20067 MS Residual=31.4534 Curvature=10.148

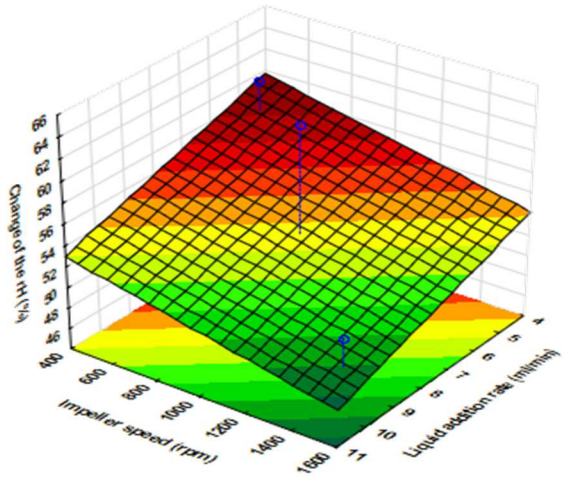

Figure 3. Relative humidity change in the kneading phase

The increasing impeller speed also decreases the general increment in the system RH%, which may indicate that; more intensive mixing promotes the uniform distribution of moisture, which increases the amount of the surface adsorbed fraction. Nevertheless, at a lower impeller speed, RH% was comparable in the entire granulation chamber, but the increasing impeller

speed resulted in greater RH% variation with a rapid increase in RH% values throughout the granulation chamber. This may be due to the increased evaporation rate in the elevated temperature regions, which is supported by the similar distribution of temperature and RH% values. The results confirmed the original hypothesis that there are differences in the distribution of T and RH% inside the granulation chamber, which may result in the formation of hot spots, which represent the critically degrading microenvironment for sensitive drugs.

5.2. Investigation of the impact of material attributes

The CM has big columnar/tabular crystals with sharp edges, and wide particle size distribution (Figure 4c), while SDM has spherical particles with narrower size distribution (Fig. 4d), which may be considered as aggregates of columnar microcrystals. A further difference that; while CM is pure β form, SDM is a mixture of α and β forms, which exerted smaller elasticity in compression studies.

The detected maximum temperatures (Figure 5) are good indicators of material behavior during the kneading phase. It is clearly visible that at low shear rates (processes 1 and 2) there is no difference in the recorded temperature. In contrast, at high levels of impeller speed and low levels of liquid addition, C2 exhibited considerably lower maximum temperature compared to C1 and C3. *Schaefer and Mathiesen* 1996, reported that; the increase in T in high shear granulation is mainly attributed to the conversion of the mechanical energy input into the heat of friction within the moist mass. Therefore, the lower temperature elevation upon high mechanical attrition may be due to the better deformation properties of SDM over CM.

The T excess arising in the case of C1 may be compensated by the cooling effect of an increased liquid addition rate as long as it is related only to the presence of CM. However, if CM is combined with lyso-2 in C3, the further increasing friction results in a much higher T than a composite containing SD lyso-1 (C1 and C2), despite the increased liquid addition rate. In conclusion, in spite of the general physicochemical similarities and the similar liquid uptake pattern (0.6 ml/g) of the SD and C form of raw materials, the material attributes showed obvious differences in thermal behavior upon the applied mechanical stress, especially at higher shear rates. This finding is supported by *Hulse et al.2009,* who reported that; despite the similarity in the thermal behavior of CM and its different forms such as SDM, a full characterization is required as a preformulation step because these polymorphs are dissimilar in their physical properties Tables 4-6.

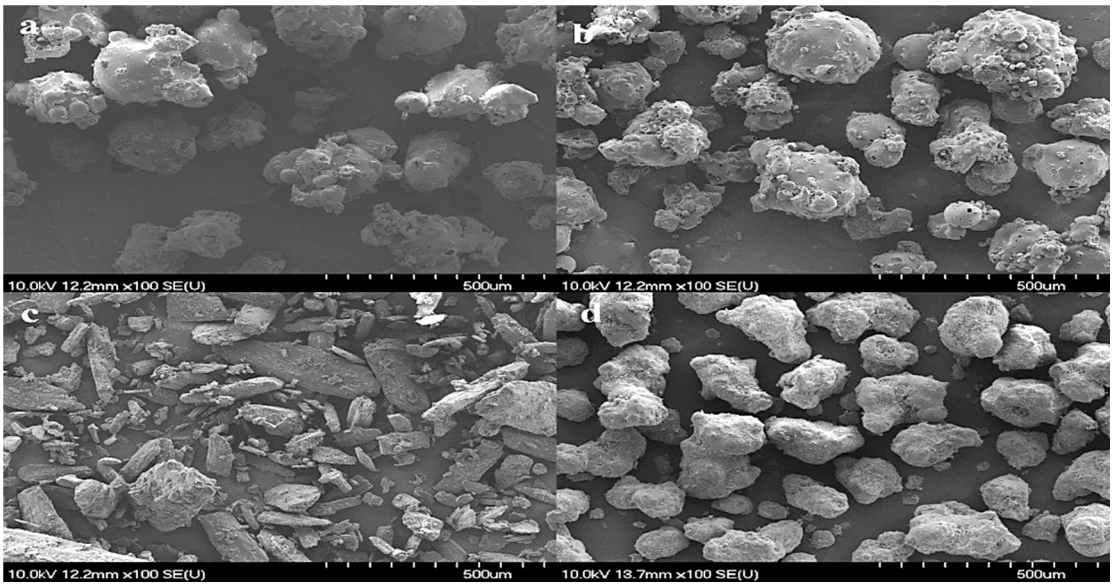

Figure 4. Scanning electron micrographs of lyso-1 (a), lyso-2 (b), CM (c) and SDM (d)

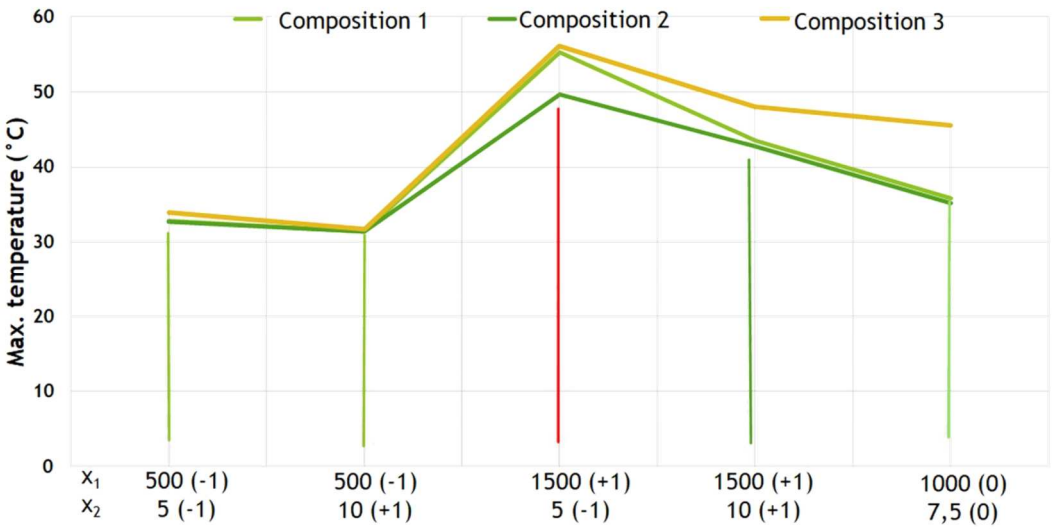

Figure 5. Maximum recorded temperature under different processing conditions for the various compositions (C1, C2 and C3)

Table 4. Physical properties and biological activity of C-1-pellets

Sample	Activity% (y_{11})	Hardness (N) (y_{21})	MC% (y_{31})	Roundness (y_{41})	Aspect ratio (y_{51})
Lys1-11	95.92	15.55 ±1.67	0.93 ±0.02	1.13 ±1.13	1.14 ±1.10
Lys1-12	92.75	13.03 ±1.10	0.51 ±0.03	1.11 ±0.08	1.13 ±0.06
Lys1-21	88.56	13.00 ±1.17	0.62 ±0.02	1.17 ±0.10	1.18 ±0.10
Lys1-22	111.56	11.60 ±1.24	0.44 ±0.01	1.15 ±0.10	1.16 ±0.10
Lys1-31	90.68	14.64 ±1.54	0.59 ±0.02	1.15 ±0.07	1.16 ±0.07
Lys1-32	76.46	12.50 ±1.55	0.41 ±0.03	1.14 ±0.07	1.15 ±0.06
Lys1-41	96.30	14.00 ±1.05	0.63 ±0.02	1.14 ±0.09	1.14 ±0.06
Lys1-42	85.93	13.60 ±1.41	0.40 ±0.01	1.1 5 ±0.12	1.14 ±0.07
Lys1-C	88.99	14.04 ±1.05	0.77 ±0.02	1.13 ±0.10	1.13 ±0.05

Table 5. Physical properties and biological activity of C-2-pellets

Sample	Activity% (y_{12})	Hardness (N) (y_{22})	MC% (y_{32})	Roundness (y_{42})	Aspect ratio (y_{52})
Lys2-11	89.84	13.01 ±1.50	1.00 ±0.03	1.12 ±0.06	1.17 ±0.07
Lys2-12	109.96	12.33 ±1.21	0.47 ±0.02	1.12 ±0.06	1.17 ±0.08
Lys2-21	89.43	11.12 ±1.57	1.10 ±0.02	1.10 ±0.04	1.15 ±0.07
Lys2-22	97.30	10.20 ±1.53	0.82 ±0.02	1.11 ±0.06	1.17 ±0.08
Lys2-31	88.49	16.10 ±2.50	0.56 ±0.01	1.17 ±0.22	1.20 ±0.12
Lys2-32	91.91	14.44 ±2.53	0.40 ±0.01	1.16 ±0.14	1.22 ±0.10
Lys2-41	102.50	15.13 ±2.40	0.59 ±0.02	1.14 ±0.10	1.17 ±0.08
Lys2-42	103.08	13.21 ±1.50	0.42 ±0.01	1.16 ±0.16	1.20 ±0.10
Lys2-C	84.15	14.76 ±1.63	0.79 ±0.03	1.15 ±0.10	1.21 ±0.10

Table 6. Physical properties and biological activity of C-3-pellets

Sample	Activity% (y_{13})	Hardness(N) (y_{23})	MC% (y_{33})	Roundness (y_{43})	Aspect ratio (y_{53})
Lys3-11	79.00	15.23 ±1.64	0.93 ±0.03	1.17 ±0.13	1.18 ±0.11
Lys3-12	76.47	13.35 ±2.02	0.55 ±0.02	1.17 ±0.10	1.16 ±0.07
Lys3-21	84.81	15.26 ±2.10	0.94 ±0.04	1.17 ±0.13	1.17 ±0.10
Lys3-22	74.51	13.28 ±1.58	0.65 ±0.02	1.16 ±0.10	1.17 ±0.10
Lys3-31	87.18	15.95 ±2.61	0.67 ±0.05	1.16 ±0.08	1.24 ±0.10
Lys3-32	77.66	14.21 ±2.26	0.59 ±0.03	1.20 ±0.16	1.28 ±0.14
Lys3-41	92.79	12.83 ±2.18	0.97 ±0.03	1.21 ±0.14	1.22 ±0.12
Lys3-42	79.17	11.01 ±1.32	0.72 ±0.07	1.22 ±0.11	1.20 ±0.10
Lys3-C	66.67	13.77 ±1.48	0.83 ±0.03	1.24 ±0.20	1.23 ±0.10

5.3. Pellets properties

5.3.1. Biological activity

The statistically obtained equations describing the relationship between factors x_1, x_2 and x_3, and enzyme activity (y_1) are listed below Eqs. (3, 4 and5). The statistically significant factor coefficients are shown in bold, and some unnecessary elements were omitted to improve the model quality.

$$y_{11}=92.267-0.597x_1+3.314x_2-4.926x_3+3.749x_1x_2-5.550x_1x_3-2.786x_1x_2x_3 \quad (3)$$
$$_{adj}R^2=0.9814 \quad MS_{Residual}=1.667 \quad Curv.\ coeff.=-3.282$$

$$y_{12}=96.56\mathbf{+4.00x_1+1.51x_2-1.89x_1x_2-3.00x_1x_3+4.78x_2x_3+1.18x_1x_2x_3} \quad (4)$$
$$_{adj}R^2=0.9995 \quad MS_{Residual}=0.0369 \quad Curv.\ coeff.=\mathbf{-12.41}$$

$$y_{13}=81.45-4.50x_1+1.37x_2+2.75x_3-1.49x_1x_2-1.29x_1x_3+0.46x_1x_2x_3 \quad (5)$$
$$_{adj}R^2=0.9771 \quad MS_{Residual}=1.3337 \quad Curv.\ coeff.=-14.78$$

The average enzyme activity was relatively high (92.267% and 96.56%) for C1 and C2 (Eqs. 3 and 4, respectively). However, while there were no statistically significant coefficients for C1, for C2 the increment of both impeller speed and liquid addition rate significantly ($p<0.05$) increased the enzyme activity (Eq. 4). A further difference is that in the case of C1, the increasing liquid addition rate has a clearly positive effect (coefficients b_2 and b_{12}) on enzyme activity by compensating for the temperature excess caused by higher friction. In

contrast, for C2 the negative value of coefficient b_{12} indicates the negative effect of the high dosing rate when low shear rates are applied. This supports the previous conclusion made by *Sovány et al.,* 2016, that; the over-wetting of the enzyme increases its sensitivity to thermo-mechanical stress. The higher biological activity of C2 and the considerably lower enzyme activity of C3 support the argument concerning the impact of critical material attributes, especially the deformability of particles, on the quality of the macromolecular product.

5.3.2. Mechanical properties and moisture content

All the prepared samples showed fairly good breaking force (10.20 to 16.10 N), making them suitable for the subsequent coating process, which requires the granules to be hard enough to withstand the mechanical attrition encountered during the coating process.

$$y_{21}=13.49+0.195x_1-0.440x_2-0.808x_3+0.555x_1x_2+0.173x_1x_3+0.358x_2x_3 \quad (6)$$
$$_{adj}R^2=0.9654 \quad MS_{Residual}=0.0481 \quad Curv.\ coeff.=0.5500$$

$$y_{22}=13.19\mathbf{+1.528x_1-0.778x_2-0.648x_3+0.228x_1x_2-0.248x_1x_3-0.063x_2x_3} \quad (7)$$
$$_{adj}R^2=0.9999 \quad MS_{Residual}=0.0001 \quad Curv.\ coeff.=\mathbf{1.568}$$

$$y_{23}=13.89\mathbf{-0.390x_1-0.795x_2-0.928x_3-0.785x_1x_2+0.038x_1x_3}-0.023x_2x_3 \quad (8)$$
$$_{adj}R^2=0.999 \quad MS_{Residual}=0.0005 \quad Curv.\ coeff.=\mathbf{-0.1200}$$

Despite the considerably high values of the coefficients, none of the factors showed statistical significance in the case of C1 (Eq. 6). In contrast, their effects on C2 and C3 were significant (Eqs. 7 and 8). Increasing the impeller speed increases the hardness of C1 and C2 while decreasing the breaking force of C3, which indicates that increasing friction has a negative influence on the bonding ability of mechanically resistant particles. The increment of both the liquid addition rate (x_2) and extrusion speed (x_3) decreases hardness in all cases, which may be related to the less uniform distribution of water and particle density, which considerably influences the internal texture of the pellets. The deformation of the pellets starts with a viscoelastic deformation to the increasing load, followed by a plastic deformation as shown below (Fig. 6). In some cases, a multi-stage deformation process was observed (Fig. 6b). However, some particles illustrated more than one peak at the viscoelastic phase may be attributed to the presence of microfractures due to small inconsistencies or structural defects in the pellet texture.

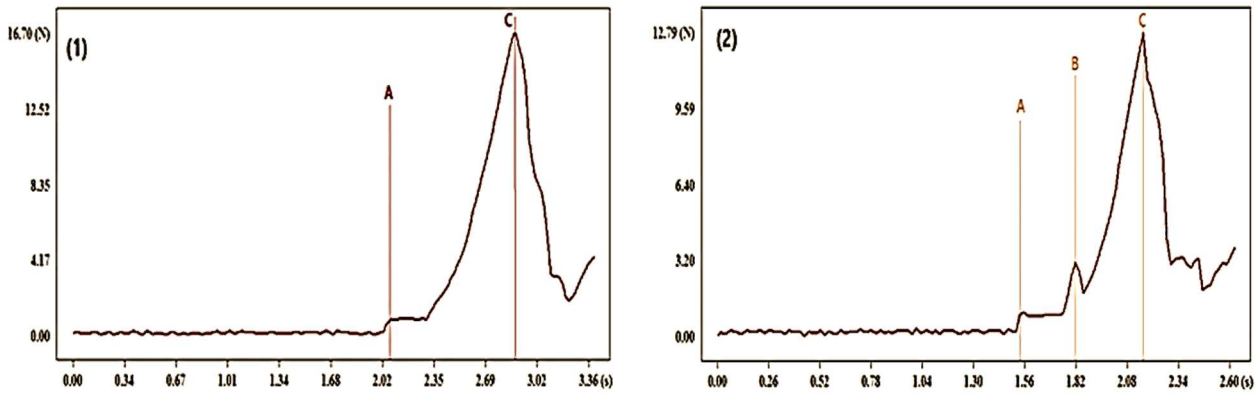

Figure 6. Typical pellet deformation curves, A and B: viscoelastic stages of deformation and C: the final plastic deformation step

The physical interactions upon liquid (water) addition and mixing were almost similar for all formulations (C1-C3) processed under the same experimental conditions and confirmed by the comparable moisture content of the formulations processed under the same conditions. In case of C1 and C2, a weaker model quality was observed, which may be related to the higher values of curvature coefficients of these compositions, which indicates certain nonlinearity of the effect of the factors. The most considerable effect was exerted by the extruder speed (x_3), but it was found significant only for C1 (Eq. 9). The results indicate higher extrusion rates may repulse water from the wet mass and so decrease the final MC of the pellets.

$$y_{31}=0.566-0.059x_1-0.044x_2\mathbf{-0.126x_3}+0.051x_1x_2-0.036x_1x_2x_3 \quad (9)$$
$$_{adj}R^2=0.8544 \quad MS_{Residual}=0.0045 \quad Curv.\ coeff.=0.2038$$

$$y_{32}=0.670-0.178x_1+0.063x_2-0.143x_3-0.050x_1x_2+0.060x_1x_3-0.033x_1x_2x_3 \quad (10)$$
$$_{adj}R^2=0.8899 \quad MS_{Residual}=0.0072 \quad Curv.\ coeff.=0.1200$$

$$y_{33}=0.753-0.015x_1+0.068x_2-0.125x_3+0.040x_{1x2}+0.043x_1x_3-0.033x_1x_2x_3 \quad (11)$$
$$_{adj}R^2=0.9688 \quad MS_{Residual}=0.0008 \quad Curv.\ coeff.=0.0775$$

Generally, the moisture content of all the prepared samples was good (max. 1.1%) and could be maintained under appropriate packaging and storage conditions.

5.3.3. Roundness and aspect ratio

The roundness of all the produced samples of C1 and C2 was good (<1.2), while C3 showed slightly higher values (≤ 1.28). As known, the closer roundness is to 1, the closer the sample shape is to circular, thus allowing pellets to be coated effectively. The liquid addition rate had a significant effect on pellet roundness for C1 and C2 (Eqs. 12 and 13). Interestingly, the increasing liquid addition rate increased the roundness of C1 and C3, while decreasing the roundness of C2. This could be attributed to the different material characteristics, especially to the different deformation characteristics of SDM. The fact that impeller speed affected

roundness significantly only for C2 and the significance of the curvature coefficient of the same composition indicate that the uniformity of liquid distribution had a significant impact on the sphericity of C2. Impeller speed also had a significant effect on the AR of C2 and C3 (Eqs. 16 and 17), it was directly proportional to AR, and the interaction of the tested factors was not significant.

$$y_{41}=1.143+\mathbf{0.010x_2}-0.005x_3-\mathbf{0.010x_1x_2}+0.005x_1x_3 \quad (12)$$
$$_{adj}R^2=0.8252 \quad MS_{Residual}=0.00005 \quad Curv.\ coeff.=-0.013$$

$$y_{42}=1.135+\mathbf{0.023x_1-0.008x_2+0.005x_2x_3}+0.003x_1x_2x_3 \quad (13)$$
$$_{adj}R^2=0.9733 \quad MS_{Residual}=0.00002 \quad Curv.\ coeff.=\mathbf{0.015}$$

$$y_{43}=1.183+0.015x_1+0.005x_2+0.005x_3+0.010x_1x_2+0.008x_1x_3-0.005x_2x_3 \quad (14)$$
$$_{adj}R^2=0.9419 \quad MS_{Residual}=0.00005 \quad Curv.\ coeff.=0.058$$

$$y_{51}=1.15+0.005x_2-0.005x_3-0.013x_1x_2+0.003x_1x_3+0.003x_1x_2x_3 \quad (15)$$
$$_{adj}R^2=0.9072 \quad MS_{Residual}=0.00003 \quad Curv.\ coeff.=-0.0200$$

$$y_{52}=1.181+\mathbf{0.016x_1}-0.009x_2+0.009x_3-0.004x_1x_2+0.004x_1x_3+0.004x_2x_3 \quad (16)$$
$$_{adj}R^2=0.9774 \quad MS_{Residual}=0.00001 \quad Curv.\ coeff.=0.0275$$

$$y_{53}=1.203+\mathbf{0.033x_1}-0.013x_2-0.013x_1x_2-0.005x_2x_3-0.001x_1x_2x_3 \quad (17)$$
$$_{adj}R^2=0.9376 \quad MS_{Residual}=0.0001 \quad Curv.\ coeff.=0.0275$$

5.4. Characterization of chitosan solutions/films

MFFT was less than 15 ℃ for all investigated compositions as shown below in Table 7. This confirms the applicability of the compositions for the coating/subcoating of protein-containing solid dosage forms since the low MFFT enables to perform a failureless coating process under gentle temperature conditions (between 30–45 ℃), which may generally decrease the risk of temperature-induced misfolding of the processed polymers.

The thicknesses of the prepared films are shown in Table 7. The plasticizer-free AA-based chitosan films showed the least thickness (0.07 mm), in accordance with the literature. The thickness of CA-based chitosan films was minimum the double and proved to be directly proportional to the CA concentration (0.13–0.27 mm), indicating dilatation in the polymer backbone as a result of cross-linking by CA. The addition of a plasticizer also increases the film thickness up to a certain limit in the order of G<PG<<PEG-400 in all cases (Table7).

Table 7. Physical properties of the various chitosan solutions/films

AA (v/v%)	CA (w/v%)	Plasticizer	Plasticizer content (w/v%)	MFFT (°C)	Thickness (mm)	Hardness (N)	Mucoadhesion (N)	MC (w/w%)
2	-	-	0	<15	0.07 ± 0.02	44.63 ± 3.4	42.30 ± 3.60	01.20 ± 1.70
2	-	G	5	<15	0.21 ± 0.04	2.39 ± 0.9	9.00 ± 4.62	13.83 ± 3.64
2	-		10	<15	0.32 ± 0.10	2.91 ± 1.1	8.34 ± 1.63	11.15 ± 0.54
2	-	PG	5	< 15	0.33 ± 0.01	6.66 ± 0.71	19.49 ± 3.20	06.41 ± 2.34
2	-		10	< 15	0.13 ± 0.02	6.81 ± 0.72	10.37 ± 2.27	07.80 ± 1.90
2	-	PEG 400	5	< 15	0.21 ± 0.01	20.88 ± 1.7	13.68 ± 3.40	7.92 ± 2.71
2	-		10	< 15	0.43 ± 0.03	18.48 ± 1.7	8.69 ± 2.89	13.27 ± 3.96
-	2.5	-	0	< 15	0.13 ± 0.01	36.01 ± 3.70	47.57 ± 3.03	0.75 ± 1. 26
-	3	-	0	< 15	0.15 ± 0.10	35.65 ± 3.36	35.41 ± 2.22	0.86 ± 2.54
-	3.5	-	0	< 15	0.14 ± 0.01	48.52 ± 0.50	42.68 ± 3.10	1.14 ± 3.34
-	4	-	0	< 15	0.16 ± 0.04	32.83 ± 4.78	41.10 ± 2.93	1.99 ± 2.82
-	5	-	0	< 15	0.23 ± 0.02	39.20 ± 5.40	30.32 ± 1.84	1.05 ± 2.46
-	7	-	0	< 15	0.27 ± 0.02	8.40 ± 1.98	25.65 ± 3.90	9.15 ± 3.84
-	2.5	G	5	< 15	0.17 ± 0.02	1.04 ± 0.27	14.52 ± 1.28	0.86 ± 3.43
-	2.5		10	< 15	0.20 ± 0.01	1.93 ± 0.89	13.71 ± 0.46	1.14 ± 3.03
-	2.5	PG	5	< 15	0.21 ± 0.01	1.39 ± 0.43	13.77 ± 1.78	1.99 ± 2.50
-	2.5		10	< 15	0.22 ± 0.01	4.95 ± 0.68	9.91 ± 2.18	1.05 ± 0.92
-	2.5	PEG 400	5	< 15	0.26 ± 0.02	8.12 ± 3.95	8.67 ± 2.10	2.15 ± 1.56
-	2.5		10	< 15	0.34 ± 0.01	6..22 ± 1.92	7.86 ± 3.86	2.75 ± 2.01
-	7	G	5	< 15	0.10 ± 0.01	0.58 ± 0.64	11.07 ± 2.76	11.83 ± 4.52
-	7		10	< 15	0.14 ± 0.01	0.64 ± 0.64	13.24 ± 1.10	17.36 ± 3.67
-	7	PG	5	< 15	0.16 ± 0.01	1.33 ± 0.14	15.80 ± 0.84	8.33 ± 1.80
-	7		10	< 15	0.18 ± 0.01	1.27 ± 0.25	12.20 ± 1.22	10.46 ± 2.67
-	7	PEG 400	5	< 15	0.23 ± 0.02	2.75 ± 1.10	18.13 ± 2.57	4.55 ± 0.73
-	7		10	< 15	0.33 ± 0.02	6.22 ± 1.80	16.79 ± 1.35	3.25 ± 2.22

Plasticizer-free films made with CA in different quantities (2.5, 3, 3.5, 4, and 5 w/v %) showed a high breaking force in the range of 32.83–48.52 N, which was comparable with AA-based chitosan films. Nevertheless, a dramatic increase was observed in the time of elongation (Figure 7) due to a viscoelastic change in the texture of films, found to be proportional to the amount of CA. However, when CA reaches 7 w/v %, a sharp reduction of the hardness with a marked increase in elasticity. In conclusion, CA may be a good plasticizer for chitosan and the ideal mechanical property may be achieved when it is used in the 3.5–5 w/v % range.

As regards the hardness of films made with PEG-400, it was significantly ($p < 0.0001$) better compared to the other plasticizers. However, it is notable that the addition of PEG-400 affects hardness inversely compared to PG or G, and a further decrease in hardness was observed when the added quantity of PEG-400 was increased. In contrast, the increasing amount of PG and G resulted in a slight, but not significant increase in hardness.

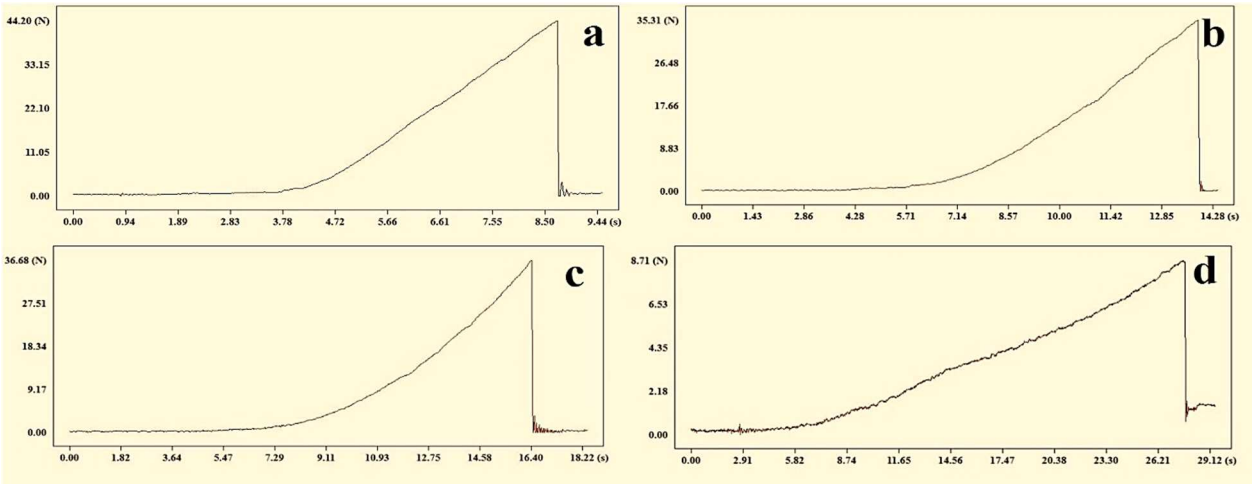

Figure 7. Breaking curves of CA 2.5% (a), CA 4% (b), CA 5% (c) and CA 7 % (d) based chitosan films

Regarding mucoadhesion, the plasticizer-free AA-based chitosan films exhibited a high force of detachment (42.30 N) (Table 7), whereas plasticizer-free CA 2.5 w/v%-based films showed even higher values (47.57 N), possibly due to the lower degree of ionization, which enables the formation of strong ionic interactions between the unionized amino groups of chitosan and the sialic acid parts of mucin molecules. In contrast, the increment of CA content or the addition of a plasticizer significantly ($p < 0.0001$) reduced mucoadhesive force (Figure 8). This could be attributed to the interactions between chitosan and the plasticizers, which decrease the number of free functional groups, or to the covering of the pores at the film surface and retarding the wetting process. Compared to the other films, CA 3.5, 4 and 5 w/v%-based films are the most applicable depending on their tensile strength and mucoadhesion in these concentration ranges, as CA showed an ideal plasticizing effect as well as a good cross-linking effect on the chitosan molecule.

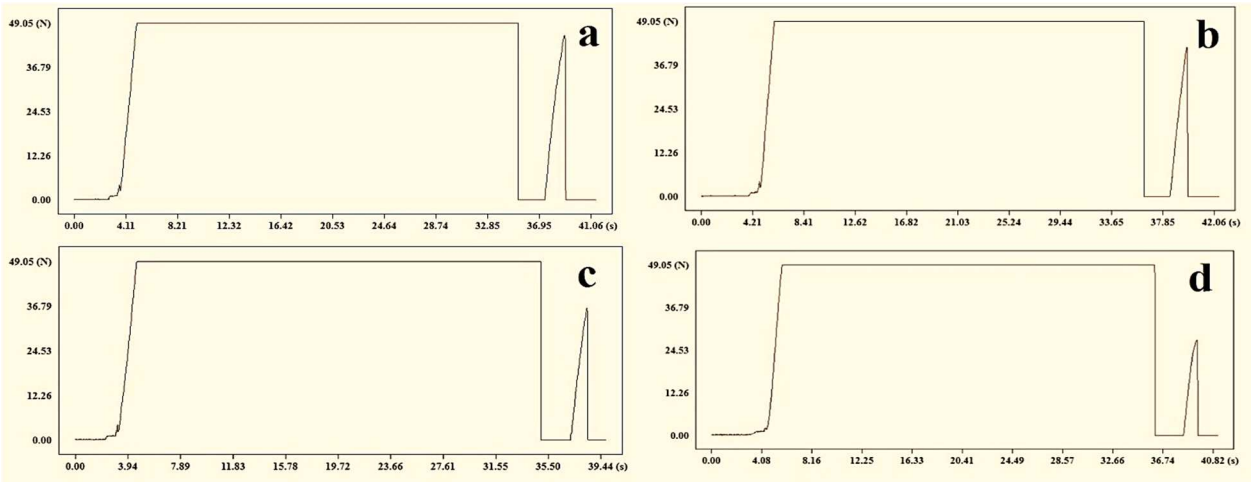

Figure 8. Mucoadhesion curves of CA 2.5% (a), CA 4% (b), CA 5% (c) and CA 7%-based chitosan films

The obtained SFEs of the prepared films are shown below in Table 8. The plasticizer-free AA-based film exhibited moderate SFE (~27 mN/m), while CA-based films showed significantly higher SFE around 40 mN/m without any considerable difference regarding the CA content. The polarity of CA-based films was also higher than that of the AA-based ones. However, the increasing CA content significantly decreased polarity, which may be related to the pH of the solution.

Table 8. SFE (γ^{total}), its dispersive (γ^{d}) and polar (γ^{p}) components and polarity of the prepared films

AA (w/v%)	CA (w/v%)	Plasticizer	Plasticizer content (w/v%)	γ^{total} (mN/m)	γ^{d} (mN/m)	γ^{p} (mN/m)	Polarity (%)
2	-	-	0	26.58 ± 2.25	14.82 ± 0.65	11.80 ± 2.15	44.40
2	-	G	5	15.55 ± 1.94	9.22 ± 0.78	6.33 ± 1.80	40.71
2	-		10	13.21 ± 1.85	8.21 ± 0.78	5.00 ± 1.70	37.85
2	-	PG	5	14.95 ± 2.12	8.12 ± 0.94	7.33 ± 1.90	49.03
2	-		10	15.75 ± 1.84	12.39 ± 0.86	3.40 ± 1.38	21.61
2	-	PEG 400	5	44.71 ± 2.74	22.38 ± 0.90	22.20 ± 2.60	49.65
2	-		10	47.30 ± 3.00	25.66 ± 1.50	22.10 ± 2.56	46.72
-	2.5	-	0	41.50 ± 1.90	18.33 ± 0.90	23.13 ± 1.70	55.73
-	3	-	0	44.31 ± 1.65	24.44 ± 0.70	19.87 ± 1.50	44.84
-	3.5	-	0	37.97 ± 1.80	17.12 ± 0.68	20.90 ± 1.63	55.04
-	4	-	0	43.34 ± 1.72	17.12 ± 0.74	20.76 ± 1.55	48.00
-	5	-	0	42.54 ± 1.71	23.98 ± 0.86	18.31 ± 1.50	43.04
-	7	-	0	39.40 ± 2.65	22.80 ± 2.01	16.59 ± 1.64	41.40
-	2.5	G	5	29.60 ± 2.02	16.54 ± 1.33	13.05 ± 1.50	44.10
-	2.5		10	27.23 ± 2.72	16.69 ± 2.01	10.54 ± 1.70	38.71
-	2.5	PG	5	47.66 ± 1.84	29.38 ± 1.12	18.30 ± 1.50	38.40
-	2.5		10	36.85 ± 1.80	19.15 ± 0.90	17.82 ± 1.54	48.40
-	2.5	PEG 400	5	57.40 ± 1.73	35.73 ± 1.00	21.70 ± 1.42	37.80
-	2.5		10	54.14 ± 1.60	35.16 ± 0.82	19.00 ± 1.33	35.10
-	7	G	5	40.10 ± 1.85	27.58 ± 1.27	12.50 ± 1.64	31.20
-	7		10	38.57 ± 1.52	24.98 ± 0.72	13.60 ± 1.33	35.30
-	7	PG	5	37.30 ± 2.04	26.78 ± 1.58	10.25 ± 1.31	27.50
-	7		10	36.63 ± 1.72	26.84 ± 1.15	9.80 ± 1.25	26.80
-	7	PEG 400	5	65.77 ± 2.11	34.37 ± 1.55	31.40 ± 1.43	47.74
-	7		10	68.11 ± 1.81	36.77 ± 1.23	31.35 ± 1.32	46.03

The addition of PEG-400 increased SFE as well as polarity, in both 5 and 10 w/v% concentrations, which may be due to the presence of polar oxygen in the PEG backbone, which will be present on the film surface after the cross-linking of the chitosan chains, or in a manner enabling the polymer to dissolve in a relatively high amount of CA, resulting in ester formation and at the same time saving some polar functional groups (OH groups) on the surfaces when the films get dry.

Overall, a plasticizer-free CA-based film may be chosen as an oral film to deliver a macromolecule, as the values of hardness and SFE were relatively adequate, while the good wetting and high mucoadhesivity enable the films to tightly adhere to the mucosal surface. However, if the film would be utilized as the subcoating of an intestinosolvent coat, the PEG plasticized film seems to be the best solution due to its higher hardness and higher SFE, which will enable better spreading and adhesion of the intestinosolvent coat on the substrate surface.

Chitosan was dissolved in AA 2 v/v% due to the ionization of the non-acetylated amide groups, as shown by the right shift of the N–H stretching and the left shift of the N–H bending absorption bands as shown in (Figure 9). The appearance of a new band at 1750 cm^{-1} indicates the esterification and hydrogen bonding of some hydroxyl groups, similarly to the right shift of the broad O–H stretching peak at 3600–3000 cm^{-1} and the left shift of the OH bending. The addition of plasticizers resulted in no considerable change in the texture, but some signs of weak hydrogen bonds were noticed in the order of G>PEG-400>PG, which may be due to the number of free hydroxyl groups on the plasticizers.

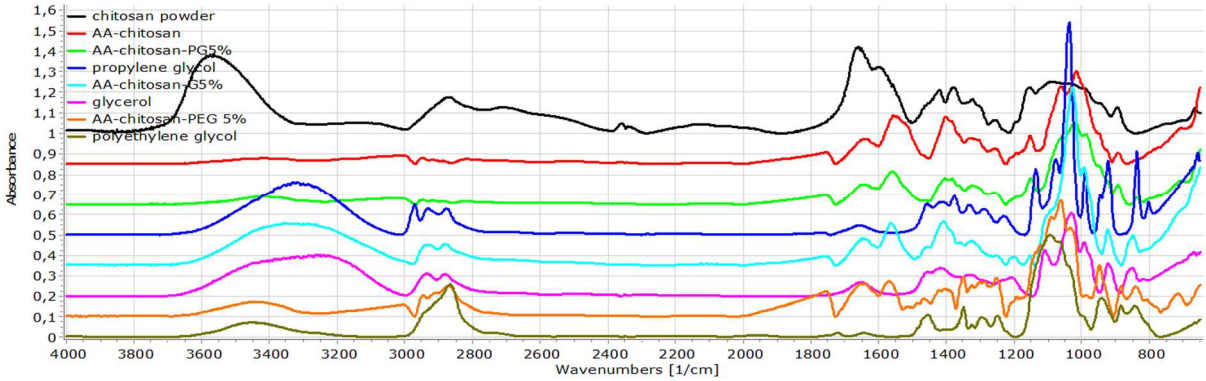

Figure 9. FT-IR spectra of raw materials and AA-based films

The FT-IR spectra of CA-based chitosan films made with varying amounts of CA (Figure 10) indicate the presence of strong H-bonds between the –OH groups of the polymer and the carboxyl groups of the acid with a right shift of the –OH stretching peak between 3600–3300 cm^{-1}. The more intensive right shift of the N–H stretching signal between 3300–3000 cm^{-1}, the stronger left shift of the NH bending at 1590 cm^{-1}, and the increasing intensity of the new broad peak at 2000 cm^{-1} indicate the stronger ionization of the amino groups with increasing CA content.

However, no considerable difference was observed between CA 2.5% (Figure 11) and CA 7% based films which indicates that; polymer-plasticizer interactions may be related mostly to the bonding of -OH groups, and therefore the increasing ionization grade of chitosan does not considerably affect the strength of these interactions. Generally, it can be concluded that the

addition of polyhydroxy alcohols such as G, PG and PEG-400 will result in the formation of weak H bonds with the hydroxyl groups of chitosan

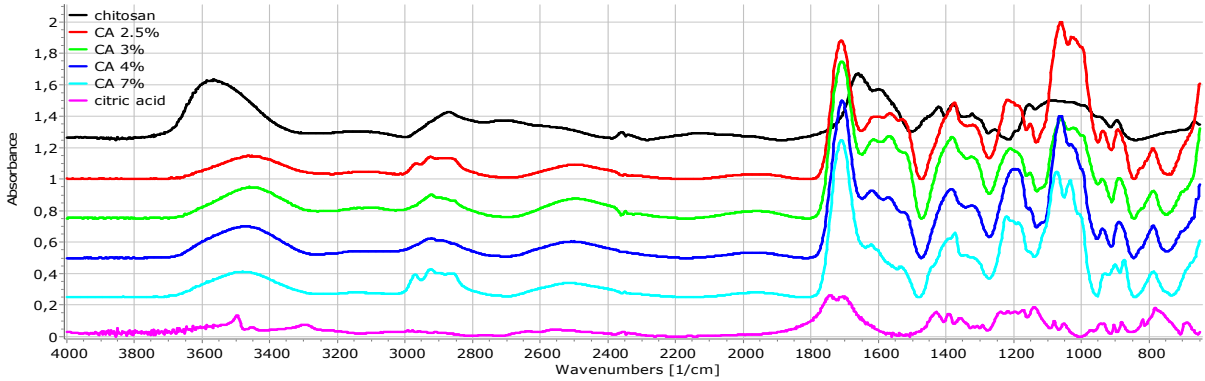

Figure 10. FT-IR spectra for 2.5, 3, 4, and 7 w/v% CA-based chitosan films

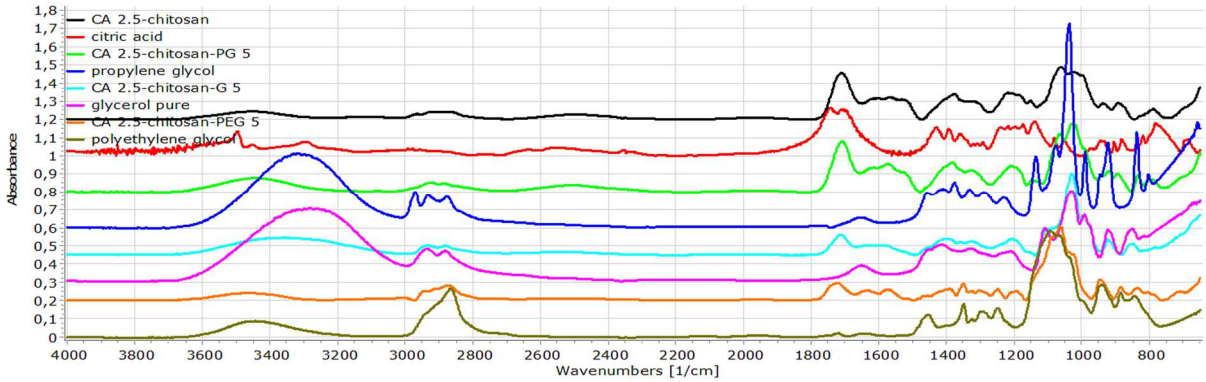

Figure 11. FT-IR spectra of raw materials and CA 2.5%w/v-based chitosan films

Regarding the thermal analysis, films made with PG had the lowest thermal stability overall compared to those made with G and PEG-400 (Figure 12). The latter showed the thermally most stable composite, which is attributed to the stability of PEG-400 (decomposition temperature of 426.2℃). Accordingly, PEG-based films are the best composites as regards long-term stability.

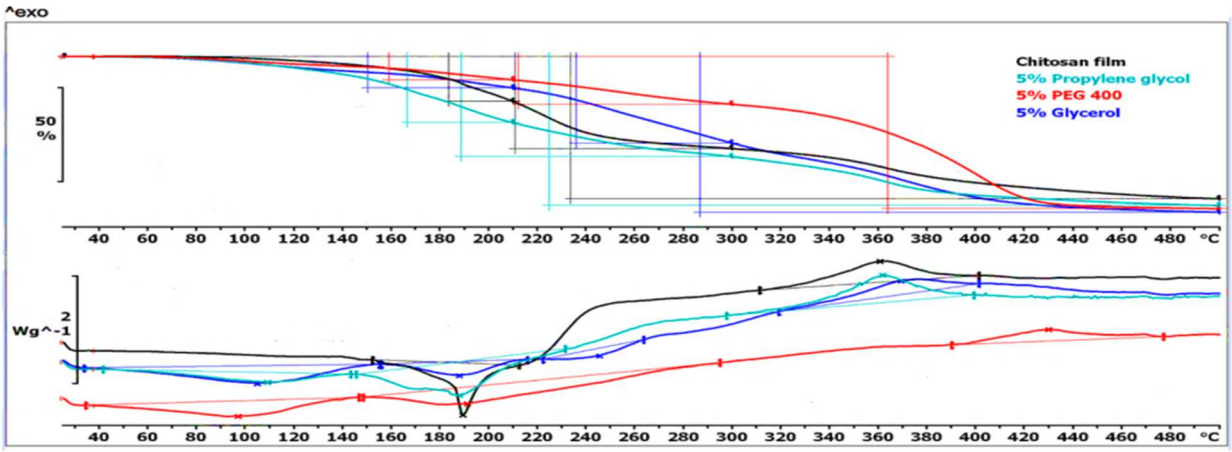

Figure 12. TG/DSC curves of 2.5 w/v% CA-based chitosan films made with/without 5w/v% of plasticizers

6. CONCLUSIONS

The present study covered the investigation of the effects of material characteristics on the design space of the production of lysozyme-containing pellets, and the development of chitosan-based films suitable for their subsequent coating process.

The results revealed that; material attributes had considerable effects on the process design space. Accordingly, the investigation of the critical material attributes during the early stage of development is essential both for APIs and excipients since they have a potential impact on the process temperature, and therefore on the biological activity of biopharmaceuticals. Nevertheless, despite their different deformability, both CM and SDM elicited a considerable conformation stabilizing property against high shear stress and allowed only reversible modification in the lysozyme structure, which was confirmed by the fact that the protein regained its active conformation and activity after a few days.

The specially designed granulation chamber represented a novel tool of process analytical technology (PAT) and quality by design (QbD). It allowed the precise monitoring of the changes in temperature and RH% during high shear kneading, helping to optimize process parameters for the requirements of macromolecular or other thermolabile drugs.

The results also confirmed the importance of the chamber wall material, since the granulation chamber made from Teflon demonstrated a lower temperature upon elevated mechanical attritions than a glass-constructed chamber because of their different thermal conductivity.

In the second phase of the study, CA-based chitosan solutions/films were intensively characterized, and their applicability as multifunctional subcoating polymers (MFFT <15° C) as well as their suitability as oral films with respect to AA-based films as a reference were successfully done. It was proven that CA-based chitosan films may be successfully prepared with the direct dissolution of the polymer in CA solution, and the obtained films exhibited properties comparable to AA-based ones. Nevertheless, CA-based films offer the possibility to tailor mucoadhesivity of chitosan and synergistically intensification of the penetration enhancing and protease inhibiting effects.

PRACTICAL USEFULNESS

The experimental work of this study has allowed the following conclusions:

Factorial design is highly essential for the design and the investigation of critical processing factors and for the good understanding of the effect of material characteristics and their impacts on the critical product quality (CPQ).

The extrusion/spheronization method of pelletization is a very good technique for the development of lysozyme-loaded pellets because of a wide range of flexibly adjustable process parameters.

Various forms of mannitol (CM and SDM) are suitable enzyme stabilizers despite the different deformability patterns.

The specially designed granulation chamber is a novel tool for precisely monitoring the temperature and RH at different locations within the chamber and for correlating the effect of applied mechanical attritions and generated temperature with the product properties.

The high shear granulator is an ideal granulation method to preserve the homogeneity of the mixtures, thus reducing batch-to-batch variation.

CA-based chitosan solutions/films cross-linked with different plasticizers produce solutions/films with properties such as mucoadhesivity and SFE. This enables the utilization of these solutions/films for various pharmaceutical applications in the development of oral mucoadhesive films, or the development of multifunctional subcoating/coating for the delivery of poorly absorbable drugs.

Financial Support

This study was financially supported by Omdurman Islamic University (OIU) in cooperation with the Higher Ministry of Education and Scientific Research, Sudan.

LIST OF PUBLICATIONS AND CONFERENCE PROCEEDINGS

List of publications related to the thesis

1. **Ibrahim, Yousif H-E. Y.**; Regdon jr., Géza; Hamedelniel, Elnazeer I; Sovány, Tamás. Review of recently used techniques and materials to improve the efficiency of orally administered proteins/peptides, DARU J. Pharm. Sci. 28 (2020) 403-416. https://doi.org/10.1007/s40199-019-00316-w. **Indep. citations: 17 Q2 IF (2020): 3,117**
2. **Ibrahim, Yousif H-E. Y.**; Regdon jr., Géza; Kristó, Katalin; Kelemen, András; Adam, Mohamed E.; Hamedelniel, Elnazeer I.; Sovány, Tamás. Design and characterization of chitosan/citrate films as carrier for oral macromolecule delivery, Eur. J. Pharm. Sci. 146 (2020) 105270. https://doi.org/10.1016/j.ejps.2020.105270.

   Indep. citations: 3 Q1 IF (2020): 4,384
3. **Yousif H-E.Y. Ibrahim**, Patience Wobuoma, Katalin Kristó, Ferenc Lajkó, Gábor Klivényi, Béla Jancsik, Géza Regdon jr., Klára Pintye-Hódi, Tamás Sovány, Effect of Processing Conditions and Material Attributes on the Design Space of Lysozyme Pellets Prepared by Extrusion/Spheronization, Journal of Drug Delivery Science and Technology (Accepted, 6th July 2021). **Q2 IF (2020): 3,981**

List of publications not related to the thesis

1. Hamedelniel, Elnazeer I.; Omer, Hagir M.; Balla, Qussai I.; **Ibrahim, Yousif H-E. Y.**; Osman, Fakhr Aldeen Y.; Abdelmonem, M. Abdellah. Formulation and evaluation of Grewia tenax fruits as effervescent tablets for treatment of iron deficiency anemia, Int. J. Develop. Res. 10 (2020) 34084-34090.

2. Robert-A. Vlad, Tamas Sovany, Katalin Kristó, **Ibrahim, Yousif H-E. Y.**, Adriana Ciurba, Zoltan Aigner, Daniela Muntean, Geza Regdon, Structural and Thermal Analysis of Cannabidiol Orodispersible Formulations, Pharmacia, 69 (2021) 426–433. https://doi.org/10.31925/farmacia.2021.3.5.

List of conference proceedings

1. **Ibrahim, Yousif H-E. Y.**; Regdon jr, Géza; Sovány, Tamás. Design, Development and Characterization of Chitosan Film as Effective Oral-Macromolecule Delivery System Using New Multifunctional Plasticizer. Acta Pharmaceutica Hungarica 88 (2018) 3 pp. 148-148. Paper: P4/11.

2. **Ibrahim, Yousif H-E. Y.**; Sovány, Tamás; Regdon jr., Géza. Characterization of Chitosan/citrate Films as a suitable Oral-Macromolecule Carrier, I. Ph.D. Symposium at the University of Szeged - Medical and Pharmaceutical Sciences, Szeged, November (2018).

3. **Ibrahim, Yousif H-E. Y.**; Sovány, Tamás; Regdon jr., Géza. Design and characterization of Chitosan/citrate films as suitable multifunctional coating for oral-macromolecule delivery I. Symp. Young Res. Pharm. Technol. Biotech. Reg. Sci., Szeged, Hungary (2019) pp. 15-15.

4. **Ibrahim, Yousif H-E. Y.**; Sovány, Tamás; Regdon jr., Géza. Effect of plasticizer type/quantity on the thermal behavior of acetic acid and citric Acid-based chitosan films in: 2nd Journal of Thermal Analysis and Calorimetry Conference, Budapest, Hungary Book of Abstracts (Akadémiai Kiadó), (2019) p. 653.

5. Kristó, Katalin; **Ibrahim, Yousif H-E. Y.**; Regdon jr., Géza; Sovány, Tamás. A tervezési tér optimálása lizozim tartamú pelletek előállítása során In: Gyógyszertechnológiai és Ipari Gyógyszerészeti Konferencia: A Magyar Gyógyszerésztudományi Társaság Gyógyszeripari Szervezetének és Gyógyszertechnológiai Szakosztályának Konferenciája (2019) p. 35.

6. Sovány, Tamás; **Ibrahim, Yousif H-E. Y.**; Kristó, Katalin; Regdon jr., Géza. Effect of material attributes on the design space of lysozyme containing pellets in: 8th BBBB International Conference on Pharmaceutical Sciences Abstract Book (2019) Conference Paper.

7. **Ibrahim, Yousif H-E. Y.**; Kristó, Katalin; Regdon jr., Géza; Sovány, Tamás. Effect of Processing Conditions and Material Attributes on the Design Space of Lysozyme Pellets Prepared by Extrusion/Spheronization: II. Symposium of Young Researchers on Pharmaceutical Technology, Biotechnology and Regulatory Sciences, Szeged, Hungary, 2020: pp. 39. https://doi.org/10.14232/syrptbrs.2020.op34.

8. **Ibrahim, Yousif H-E. Y.**; Kristó, Katalin; Regdon jr., Géza; Sovány, Tamás. Effect of Plasticizer Type and Quantity on the Properties of Oral Chitosan Films. EUGLOH Annual Student Research Conference, University of Szeged, 28-30th September 2020, Hungary.

9. **Ibrahim, Yousif H-E. Y.**; Kristó, Katalin; Regdon jr.; Géza; Sovány, Tamás. Development and optimization of the coating processes of lysozyme loaded pellets for oral delivery, III. Symposium of Young Researchers on Pharmaceutical Technology, Biotechnology and Regulatory Sciences. Szeged, Hungary, 2021: pp. 48. https://doi.org/10.14232/syrptbrs.2021.op36.